HHS Public Access

Author manuscript

Biochemistry. Author manuscript; available in PMC 2017 August 15.

Published in final edited form as:

Biochemistry. 2017 January 10; 56(1): 281–293. doi:10.1021/acs.biochem.6b00468.

Differential Membrane Binding Mechanics of Synaptotagmin Isoforms Observed at Atomic Detail

Josh V. Vermaas[†,‡] and **Emad Tajkhorshid**[†]

[†]Center for Biophysics and Quantitative Biology, Department of Biochemistry, and Beckman Institute for Advanced Science and Technology, University of Illinois at Urbana-Champaign, Urbana, IL 61801

Abstract

Synaptotagmin (Syt) is a membrane-associated protein involved in vesicle fusion through the SNARE complex that is found throughout the human body in 17 different isoforms. These isoforms have two membrane-binding C2 domains, which sense Ca^{2+} and thereby promote anionic membrane binding and lead to vesicle fusion. Through molecular dynamics simulations using the HMMM acclerated bilayer model, we have investigated how small protein sequence changes in the Ca^{2+} binding loops of the C2 domains may give rise to the experimentally determined difference in binding kinetics between Syt-1 and Syt-7 isoforms. Syt-7 C2 domains are found to form more close contacts with anionic phospholipid head groups, particularly in Loop 1, where an additional positive charge in Syt-7 draws the loop closer to the membrane and causes the anchoring residue F167 to insert deeper into the bilayer than the corresponding methionine in Syt-1 (M173). By carrying out additional replica exchange umbrella sampling calculations, we demonstrate that these additional contacts increase the energetic cost of unbinding the Syt-7 C2 domains from the bilayer, causing them to unbind more slowly than their counterparts in Syt-1.

Graphical Abstract

Correspondence to: Emad Tajkhorshid.

[‡]Current address: Biosciences Center, National Renewable Energy Laboratory, Golden, CO 80401

Supporting Information Available

Supplemental tables and figures are provided in the Supporting Information, which include the table of the residues with the most membrane contacts, as well as complete sequence alignments for the protein structures used relative to the Syt-7-centric numbering system used here. Additional Supporting Information includes the structures containing the average atomic membrane contacts in a compact binary form readable by VMD,[41] with the PS and PC contacts stored in the beta and occupancy fields, respectively. Rotated views of the individual components of Fig. 9 are also provided. Animations showing the complete binding trajectories for one example from each C2 domain are also provided. These animations show a view centered on the protein center of mass, showing the protein as a gray cartoon with blue, green, and red highlights indicating the different loop regions. Sidechains of relative residues 165, 167, 168, 192–194, and 228–231 are drawn in outlined stick representations, while nearby HMMM phospholipids are drawn similarly but without an outline, and the heavy atoms within DCLE molecules are yellow spheres. The Ca^{2+} ions are outlined white spheres in the animations. This material is available free of charge via the Internet at http://pubs.acs.org/.

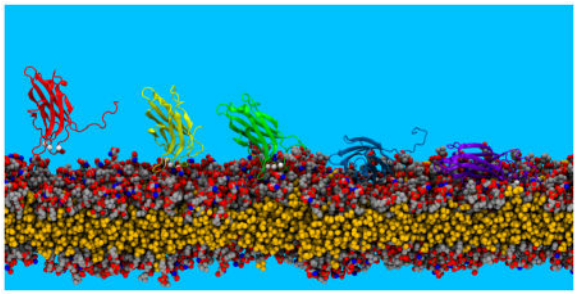

Introduction

Synaptotagmins (Syt) are peripheral membrane proteins known to play a central role in facilitating vesicle release. As part of the SNARE complex, they mediate incoming Ca^{2+} signals to trigger the fusion of vesicles to the plasma membrane and releasing vesicular contents. [2–5] There are at least 17 Syt isoforms found throughout the body, and 16 of them share the same overall topology, composed of a single transmembrane (TM) helix and two peripheral C2 domains[5] (Fig. 1). Each isoform is believed to fulfill a specific role, likely in mediating the release of vesicles containing different products (e.g., hormones, neurotransmitters) in response to a Ca^{2+} inux[5–7] by binding to anionic phospholipids on the inner leaet of the plasma membrane.[8]

These functional niches are delineated not only by cell type, but also by their required binding kinetics. Syt-1 is found primarily in nerve cells[9] and is responsible for the rapid, synchronous release of neurotransmitters after an increase in intracellular Ca^{2+} concentration brought about by an action potential.[10,11] Syt-7, in contrast, is thought to play a role in the slow, asynchronous release of neurotransmitters in the brain, as well as in Ca^{2+}-controlled release of insulin from pancreatic cells.[12–16] Experiments suggest that the functional differentiation of Syt isoforms is a result of different membrane binding modes of the peripheral Ca^{2+}–binding region of Syt,[17] known as the C2 domain, which is composed of the C2A and C2B subdomains. Despite very similar structures of the C2 domains, C2A from Syt-1 was measured to have a membrane dissociation rate that is an order of magnitude higher than the C2A domain of Syt-7.[17] Thus, the interaction between the different isoforms and the membrane seems to differ so that the bindings kinetics of each isoform matches its specific biological niche.

The molecular origins of the unique binding kinetics between the two isoforms is difficult to probe experimentally, as there are many specific changes between Syt-1 and Syt-7 C2 domains that may contribute to the overall difference. Our approach is to use the unrivaled simultaneous spatial and temporal resolutions of atomistic molecular dynamics (MD) simulations to investigate lipid-protein interactions responsible for the differential unbinding kinetics between the two isoforms,[17] and to go beyond the original experiments which focused on the C2A domains to additionally compare the binding of the C2B domains. Through MD simulations of initially unbound C2 domains placed above a bilayer, we arrive at an unbiased population of membrane-bound C2 domains for both Syt-1 and Syt-7. To accelerate lipid reorganization around the inserting C2 domains and promote rapid insertion,

we have employed the highly mobile membrane mimetic (HMMM) model.[18] The model accelerates lateral lipid diffusion and insertion by partially replacing the membrane interior by an organic solvent[18,19] while retaining an accurate energetic description of the membrane surface.[20] This approach has been used successfully to study membrane binding in other peripheral protein-membrane systems,[21–25] including a study on membrane curvature generation by the C2 domains of Syt-1.[26]

Using the HMMM model permits a thorough characterization of the interactions between each C2 domain and the membrane, including the binding depth and orientation of each C2 domain, and a comprehensive accounting of the protein-membrane contacts formed over the course of the simulations. Through this analysis, the primary difference between Syt-1 and Syt-7 is observed to occur in the C2A domains, where the number of close contacts with anionic head groups is nearly doubled in the case of Syt-7, and the residues in Loop 1 insert more deeply into the bilayer due to subtle changes in protein sequence. Through replica exchange umbrella sampling[27] (REUS) simulations, we demonstrate that these additional contacts increase the energetic cost of unbinding the Syt-7 C2 domains from the bilayer. These findings delineate how subtle sequence changes between Syt-1 and Syt-7 might substantiate their different vesicle release profiles, as the additional contacts formed between Syt-7 C2 domains and bilayer would retard unbinding and maintain the proximity of the vesicle to the membrane to which it will fuse.

Methods

Spontaneous Membrane-Binding Simulations

The basis for the simulations are a set of 20 membrane-binding simulations for each of the four isolated C2 domains to a HMMM[18] membrane composed of a 1:1 mixture of phosphatidylserine (PS) and phosphatidylcholine (PC) short-tailed lipids. This ratio was chosen to improve PS-protein interaction sampling, increasing the number of PS head groups near the protein to effectively guarantee placement of PS near any anionic binding sites. This local enrichment of PS may arise *in vivo* through PS clustering and possible domain formation by Ca^{2+} or PS binding sites on the protein itself,[28–30] and is in line with previous studies utilizing this membrane representation,[22] including prior work on Syt C2 domain conformational transitions.[26] The C2 domains were simulated independently, as the dynamics and rearrangement of the linker coupling the C2A and C2B domains is slow relative to the timescale of our simulations. The C2 domains were taken from available experimentally determined structures (Table 1).[1,31] Since the C2 domains are part of the larger Syt structure (Fig. 1), all simulations were performed with methylated neutral chain termini (ACE and CT3 patches of the CHARMM36 protein force field[32,33]) to terminate the linker stubs present in the experimental structures. Ca^{2+} was added to both C2A domains, where the structures used did not contain Ca^{2+}, by using the 4 Ca^{2+} ions of Syt-7 C2B as a template. Short, 15 ns simulations of all C2 domains in solution suggested that only 3 of the 4 ions form stable interactions with the Ca^{2+}-binding loops, and that the fourth would diffuse into solution. The additional fourth Ca^{2+} was therefore discarded, which is in agreement with the current consensus on the Ca^{2+} binding stoichiometry. [4,34] Due to the small system size, these three Ca^{2+} ions represent an approximately 4.5mM Ca^{2+}

concentration, well in excess of typical μM concentrations arising during an action potential.[35]

20 independent membranes were generated in two steps. First, a model conventional lipid bilayer was generated using CHARMM-GUI[36–38] with 70 Å side lengths, using a 1:1 ratio of PS and PC lipids and a target lipid density of 75 Å^2 per lipid. This lower density permits insertion in fixed area ensembles used in HMMM simulations[18] and has been an optimal configuration in the past. [21,22] Once the C2 domains insert into the bilayer, the domains naturally must displace some lipids, and as a result, we measure the average area per lipid at the end of simulation to be 64.6±0.3 Å^2 once this effect is taken into account. This result is approximately in line with the area per lipid measured in conventional bilayer simulations. [39] The initial full-tailed conventional membrane obtained from CHARMM-GUI was converted into an HMMM bilayer by removing the tail past C5 and placing 3 dichloroethane molecules for every 14 carbons removed in order to conserve acyl tail volume.[40] The independent membranes were combined with the C2 domains oriented with their long axis parallel to the membrane normal with their Ca^{2+}-binding loops oriented closest to the membrane approximately 5 Å distant, similar to the setup used in earlier exploration of Syt-1 C2A binding with the HMMM.[26] These systems were then solvated and ionized with the SOLVATE and AUTOIONIZE plugins within VMD[41] to a final dimension of 70 × 70 × 145 Å and a 150mM KCl concentration (Fig. 2).

Each replicate was simulated for a total of 105 ns (5 ns equilibration, 100 ns production) using NAMD 2.9[42] using the CHARMM36 protein[32,33] and lipid[43] force fields and TIP3 water.[44] During the equilibration, the protein backbone heavy atoms were harmonically restrained to their initial positions with a 0.1 kcal/mol/Å^2 force constant. This restraint was lifted for production simulations. Non-bonded forces were calculated with a 12 Å cutoff (10 Å switching distance). Long-range electrostatic forces were calculated using the particle mesh Ewald method.[45,46] A Langevin thermostat using $\gamma = 1$ ps^{-1} maintained the system temperature at 310 K. Pressure was maintained at 1 atm along the membrane normal using a Nosé-Hoover piston[47,48] with period and decay of 200 fs in a fixed area ensemble. The fixed area ensemble is required by the low surface tension of the surfactant-like, short-tailed HMMM lipids.

Analysis

In a comparative study such as this one, it is critical to establish the alignment of different elements between the C2 isoforms. While the sequence similarities are quite high (Table S1), the sequence lengths differ between species, leading to potential confusion with respect to which numbering scheme to use. For consistency, the residue numbers reported here are all with respect to the sequence alignment of Syt-7 found in humans (Figs. 3 and S19). This “relative” residue numbering is used to align the C2 domains within our analysis, and is used consistently throughout the text. To convert from this “relative” residue numbering to the actual residue position in Syt-1, add 6 or 7 to the relative residue, depending on its position in the sequence. Specifically, add 6 prior to relative residue 208, and 7 after relative residue 208.

Many analyses performed using VMD,[41] such as measuring root mean square deviation (RMSD) or membrane penetration depth, are widely used in the field, and are simple geometric analyses. However membrane penetration depth alone did not adequately delineate the role of the anionic PS head groups, so we have also included a "native contacts" measurement using the same formulation originally used for protein folding studies.[49] Specifically, given a distance x between a heavy atom in the C2 domain and a heavy atom in the lipid, we have defined a contact (C) as:

$$C(x)=\frac{1}{1+\exp\left(5\,\text{Å}^{-1}\left(x-4\,\text{Å}\right)\right)} \quad (1)$$

In this definition, a heavy atom distance of 3 Å is a nearly full contact (~ 1), a 4 Å distance is half a contact, and 5 Å is almost not a contact. All distances above 5 are 0 because of how contact pairs were initially isolated to make the computation tractable, which has a negligible impact on the sum. In this manner, close contacts, indicative of stronger interactions, are weighted more heavily than weaker contacts that are more distant and contribute less to the overall stability. However, since weaker contacts are more numerous, they also can contribute substantially to the sum, particularly for bulky hydrophobic side chains such as phenylalanine or tryptophan. This coordinate effectively replaces a traditional cutoff-based contact, and has previously been used to evaluate contact specificity in other peripheral protein systems.[22] This definition can also be used to isolate the identity of specific atoms involved in the interaction, a feature we will exploit in our exploration of Syt C2 membrane binding.

Replica Exchange Umbrella Sampling

In order to go beyond the qualitative description of membrane-protein interactions, replica exchange umbrella sampling[27] simulations (REUS, also called hamiltonian replica exchange[50] or bias exchange umbrella sampling[51,52]) were conducted to determine the binding free energy profile of each C2 domain to the bilayer, using a methodology similar to that applied recently to membrane transporter systems.[51,52] The chosen reaction coordinate is critical for these simulations, and ideally the system should have well-separated states along the reaction coordinate. Thus using the z-coordinate of the center of mass, as is common for computing the free energy profile for traversal across the membrane,[20] is inappropriate for this system due to its dependence on the orientation of the C2 domain causing discontinuous sampling, a problem which has been noted in other systems.[53] Using the contact formulation from Eq. (1) as inspiration, the contact number between the membrane and C2 domain was used as the reaction coordinate, as implemented by the collective variables (colvars) module[54] of NAMD.[42]

$$C\left(g_1,g_2\right)=\sum_{i\in g_1}\sum_{j\in g_2}\frac{1-\left(|x_i-x_j|/10\text{Å}\right)^8}{1-\left(|x_i-x_j|/10\text{Å}\right)^{16}} \quad (2)$$

Here, g_1 is the set of phosphorus atoms in the membrane, and g_2 is the set consisting of both protein Cα and side chain oxygen or nitrogen atoms, and the contact sum changes with the distances between them. The functional form of Eq. (2) differs from that of Eq. (1) due to details in implementation and computational efficiency. As implemented, the colvars module[54] computes the value of the collective variable on a single processor, meaning that overall simulation performance for collective variables that use many atoms will suffer tremendously as a result of Amdahl's Law.[55] Thus our reaction coordinate must simultaneously result in an unbound structure as the number of contacts goes to zero while minimizing the number of atoms involved in its definition. Therefore, in addition to a longer cutoff, in the REUS simulations only one atom from each lipid is used in the contact definition, and most of the atoms in the C2 domains do not contribute to the sum.

The REUS simulations were carried out with 40 umbrellas per C2 domain to describe the reaction coordinate. The replicas were initially tested for 250 ps using an equidistant distribution of replicas across the reaction coordinate, ranging from 0 (unbound) to the maximum value observed during the spontaneous membrane-binding simulations. From these short simulations, approximately equally spaced optimized umbrella centers were determined using the method of Sabri Dashti and Roitberg.[56] Since the collective variable space spanned ($0 \leq C \leq C_{max}$) differed between isoforms (Syt-7 C2 domains tended to have more contacts than their Syt-1 counterparts), the force constant used to bias each umbrella varied from between 0.005 and 0.01 kcal/mol·contact number^2, depending on the spacing between adjacent umbrellas. The force constants were chosen such that the bias relative to adjacent windows would be approximately equal, and thus the exchange ratios themselves were consistently between 0.3 and 0.5. Initial positions for each umbrella were taken from the ensemble of 20 membrane-binding simulations at a time when they were particularly close to the bias center for the contact number collective variable, which minimizes the equilibration period required. Since there are twice as many umbrellas as binding simulations, each binding simulation provided exactly two initial positions, one closer to the unbound side of the reaction ($C < \frac{C_{max}}{2}$), and one closer to the fully bound state ($C > \frac{C_{max}}{2}$). Due to their rapid convergence of the free energy profile relative to conventional umbrella sampling simulations,[52,57] REUS simulations were carried out for 10 ns per window using the same force field used for the binding simulations. In this case, 10 ns was sufficient to identify the free energy trends, and bracketed each C2 domain isoform with a unique unbinding free energy. The free energy profile and associated error bars were estimated using bayesian reweighting combined with gibbs sampling, based on the work of Habeck[58] and Bartels [59] to deconvolute the underlying free energy from the biased simulation. The methodology is definitively described in a recent work by Moradi and Tajkhorshid [60], and reformulates the traditional weighted histogram analysis method (WHAM)[61] in probabilistic terms.

Results and Discussion

There are three primary avenues of results: (1) general characterization of the binding depth and orientation of C2 domains after insertion, including experimental comparisons; (2) a specific enumeration of the interactions formed between each C2 domain and the anionic

lipid bilayer; and (3) a determination of the free energy of unbinding for Ca^{2+}-bound C2 domains. Each of these results will be discussed in turn in the sections that follow.

Binding Depth and Orientation

As we start from unbound C2 domains, our first observation is that of the binding process of the domains to the membrane (Figs. S1–S4). The kinetics of the binding process have been intentionally accelerated by using the HMMM membrane representation, so our first interest is to measure when the ensemble of trajectories can be considered bound and at equilibrium for further analysis. We find this time through the use of the Kolmogorov-Smirnov statistic,[62] which permits us to ask the question of if two distributions are different ($p < 0.05$) or similar ($p > 0.05$). For our purposes, we are interested in comparing the binding depth over time relative to the depth at the end of the simulations (Fig. 4A), and in the contact number over time relative to the distribution of contacts at the end of the simulation (Fig. 4B), both of are not demonstrably different. Additionally, we can apply another statistical test that tests for equality, such as the two one-sided T-test (TOST).[63] This test permits us to check if the mean at a given time is equivalent to a reference distribution (Figs. 4C and 4D). After approximately t=60 ns, $p < 0.05$ the vast majority of the time, indicating that the distribution mean drifts within a single standard deviation after this point. The statistical tests reinforce what is seen by eye from the individual depth or contact trajectories (Figs. S1–S8), in that the observables of interest are similar to the end state after approximately 60 ns. This time cut will be used in further analysis as the border between the insertion phase and what we judge to be equilibrium.

An early hypothesis as to the mechanism underlying the observed difference in kinetics between the C2A domains of Syt-1 and Syt-7 was that the different sequences between the two isoforms caused Syt-7 to embed deeper into the bilayer. This hypothesis, at least with respect to the C2A domains originally studied,[17] is supported by the observed insertion depths computed from our trajectories (Fig. 5 and Table 2). Loops 1 and 3 were observed to insert into the membrane, with Loop 3 inserting deeper than Loop 1 such that the center of mass was below the phosphorus plane. Insertion of Loops 1 and 3 is consistent with available experimental observations.[64,65] Within the simulations, Loop 2 and the termini of each C2 domain come into contact with the membrane, however they generally do not insert into it, with all residues remaining beyond the membrane phosphorus plane on average. In general, we measure the mean loop penetration depths for Syt-7 to be 1–2.5 Å deeper than those for comparable C2 domains in Syt-1 (Table 2). The deeper mean penetration of Syt-7 C2B is expected to increase the energetic barrier to dissociation of the domain from the membrane.

The different penetration depths measured in our simulations are broadly consistent (Fig. 6) with available membrane penetration measurements of independent C2 domains using site-directed spin-labeling.[64–66] The uncertainties in the experimental models can be significant, on the order of a few Å. It is experimentally challenging to measure insertion depth,[67] and computationally there is a wide variety of depths reported for each residue in our ensemble of simulations (Fig. 5A). Despite these challenges, for C2A domains, the trendline has a slope near 1 and an intercept that is small, suggesting that the HMMM is reasonably

representing the mean behavior of the insertion depths, potentially overestimating the membrane penetration depth by only 1–2Å in a systematic fashion. We ascribe this systematic error to the lower membrane density of the HMMM allowing slightly deeper penetration into the membrane relative to experiment. By comparison, a full membrane simulation for Syt-7 C2A has an intercept of -4Å, suggesting shallower membrane penetration, and larger slopes.[68] These findings highlight how slow conventional membrane binding simulations arrive at an inserted conformation, since the lipids are slow to move out of the way of the inserting species.[19] For C2B, where penetration depth data only exist for Syt-1, we see two subtrends corresponding to the two loops selected for experimental depth comparisons, whose slope is less than one. The slope below unity indicates that the simulation geometries and the experimental model diverge, and that one model is tilted more with respect to the membrane than the other. It should be noted that the experimental insertion model for C2B is based on fewer measurements than the model in C2A, and the spin labeled C2B domains had reduced affinity to the membrane,[65] increasing the uncertainty in the orientation.[67]

In this study, the C2A and C2B domains were simulated independently from one another; however, the height for each residue above the membrane (Fig. 5A) is nearly continuous between C2A and C2B. EPR experiments and crystal structures have suggested that C2A and C2B may bind to opposite bilayers in an anti-parallel arrangement. [69,70] Our simulations suggest that both ends of linker that would otherwise connect C2A and C2B are drawn to the membrane surface, and that a parallel orientation of the two C2 domains may also be possible, consistent with the observed synergistic membrane binding of C2A and C2B in separate experiments,[71] and with recent dimer simulation results,[72] although the nature of the simulations performed cannot address this question directly.

Indirect measures also support a parallel orientation for both C2 domains relative to the membrane normal. In measuring the tilt angles relative to the membrane normal (Fig. 7), we observe that the C2 domains of each isoform have similar distributions to one another, but different distributions between isoforms, with Syt-1 tilting more than Syt-7. Mechanistically, the increased tilt is due to the polybasic strand of Syt-1 forming better interactions with the anionic PS head groups, as specific amino acid replacements common to C2 domains of Syt-7 (see positions 185 and 318 in Fig. S19) are less drawn to the membrane and thereby induce a smaller tilt. The polybasic strand overall does not embed deeply into the membrane, thus resulting in few contacts. (Fig. 8). As a result, we observe no strong relationship between the tilt and the contact number for any isoform (Fig. S13). This is in part a result of the wide distribution of tilts observed, which are all part of the ensemble of bound states for Syt C2 domains (Figs. S9–S12). The similarity of tilt angles for C2 domains of the same Syt isoform might simplify the formation of contacts between adjacent C2 domains, such as those that have been measured via AFM and FRET in Syt-1,[73] by having compatible tilts that would maximize the interfacial area between them and promote contact formation. However as the binding kinetics of Syt-7 constructs with both a C2A and a C2B domain are independent of linker length,[74] suggestive of no contacts between C2 domains, it is unclear how prevalent interdomain contacts are in Syt isoforms in general.

Synaptotagmin Membrane Contacts

Based on the simulation design, we cannot directly measure contacts between adjacent C2 domains; however, we can explore the contacts made to the membrane. Like the membrane penetration depth, the total membrane contacts over time for the ensemble of trajectories shows the greatest change prior to t=60 ns (Figs. S5–S8). Through this exploration, we observe a trend that the mean number of contacts, as defined by Eq. (1), increases going from Syt-1 to Syt-7 (Fig. 8 and Table S2), consistent with the observed slower unbinding for Syt-7.[17] The distribution of the contacts is heavily weighted towards the loops and the polybasic strand located just before Loop 2 in the sequence, with other regions of the C2 domains contributing minimally to the overall sum. In C2A, the difference in the contact number comes primarily from Loops 1 and 2, while in C2B, the contact number differential is largest for Loop 3 (Table S3). The contribution of the polybasic strand is generally consistent between Syt-1 and Syt-7, but not between C2 domains. This suggests that the loop regions are primarily responsible for observed differences in binding kinetics between Syt-1 and Syt-7, as is visible in the localization of the contacts in Fig. 9. The increase in contacts has both hydrophobic and hydrophilic origins. Specific interactions between the loops and the membrane will be detailed in the following paragraphs.

Loop 1 of C2 domains is characterized by two aspartic acids involved in Ca^{2+} binding, but a more important sequence difference for membrane binding precedes the aspartates in the sequence. In the Syt-7 C2A domain, there are two major replacements relative to Syt-1 at positions 165 and 167 that contribute to substantial contact differences (Table S2). K165 in Syt-7 C2A will be drawn to the anionic membrane through interactions that are primarily with the hydrophyllic head groups of the phospholipids. This, in turn pushes the F167 side chain of Syt-7 C2A deeper into the membrane relative to the methionine it replaces in Syt-1, forming more contacts with the lipid tails (Fig. S14). The bulk of F167 itself also contributes, as its size can foster more nonspecific interactions deeper within the membrane. For C2B domains, there were modestly more contacts made by Syt-1 to the membrane, a result of a lysine at position 295 rather than an alanine as in the other tested C2 domains. Since this replacement happened further upstream at a position more distant from the membrane, it had a smaller effect than the substitution in C2A.

The trend for Loop 2 is that it makes fewer contacts with the membrane than Loop 1 or 3 do, which is why Loops 1 and 3 and not Loop 2 are found to penetrate the membrane experimentally.[64,66,73,75,76] However in the C2A domain of Syt-7, Loop 2 makes approximately twice as many contacts to PS as it does in any other C2 domain (Table S3). Loop 2 of the C2A domain of Syt-7 has three consecutive basic residues, and these all form direct contact with membrane phospholipid head groups (Fig. S15). In the C2A domain of Syt-1, by contrast, a histidine residue occupies position 192 rather than the lysine in Syt-7, and it remains distant from the membrane during the simulations (Fig. 10). Again, Syt-7 specific sequence changes introduces a new point of contact with the membrane, which further amplifies the membrane interactions of neighboring residues.

The Ca^{2+}-binding Loop 3 forms additional anionic contacts in both C2 domains of Syt-7 through the selection of a different basic residue at a single position. In both Syt-1 and Syt-7, there is a basic residue at position 231, a lysine in Syt-1 C2 domains, and an arginine in

Syt-7. The diffuse positive charge of the arginine forms additional interactions with surrounding anionic phospholipids, at times interacting simultaneously with both the glycerol and phosphate groups of a single PS head group, and at other times forming multidentate interactions between two separate phospholipids (Fig. 10). The charge of lysine in Syt-1 is more compact, and multiple simultaneous interaction partners would repel one another electrostatically over the comparatively short distance. Conversely, arginine is known to be able to form more interactions with anionic membranes, particularly multidentate hydrogen bonds to oxygen atoms within the phospholipids.[77,78] The additional contacts from the arginine in Syt-7 drive other residues in Loop 3 to form closer contacts with the membrane (Fig. S16). This is particularly clear for F229 from which has many more deep contacts with PS lipids in Syt-7 than in Syt-1 due to the arginine rather than lysine upstream in the sequence.

The membrane contacts do not change the overall structure of the individual C2 domains, with typical RMSD of the backbone of the beta sheets on the order of 1 Å, although larger deviations are observed for the C2A domain of Syt-7 (Fig. 11A). That is not to say that the C2 domains are static entities, as there are sporadic structural changes that occur during simulation, particularly for Syt-7 (Fig. 11B). These are primarily localized to the loop regions of the protein (Fig. 11C). The largest changes occur in the C2A domain of Syt-7, where Loop 2 rotates as it comes into contact with the membrane relative to the starting point in the solution NMR structure with no Ca^{2+} bound (Fig. 11).

The Role of Ca^{2+} in Unbinding

Taken as a whole, the additional contacts formed between Syt-7 and the membrane through the specific substitutions listed above are qualitatively consistent with the observed slower unbinding kinetics of the C2A domain of Syt-7 relative to Syt-1.[17] REUS calculations supplement this qualitative understanding with a quantitative assessment of the free energy cost associated with membrane unbinding for the bound poses obtained from the unrestrained binding simulations (Fig. 12), which correlate to the number of contacts observed in equilibrium simulation (Fig. S18). The unbinding free energies are clearly higher for Syt-7 C2 domains, suggesting again that the Syt-7 C2 domains form stronger interactions with anionic membranes than in Syt-1. If we convert these calculated unbinding free energies into membrane binding affinities, the C2 domains of Syt-1 would have membrane binding affinities of approximately 10 and 700nM for C2A and C2B respectively, compared with 50 and 10pM for Syt-7. These membrane-binding affinities are uniformly lower than the measured Syt ion-binding affinities on the μM range for Ca^{2+},[79,80] which suggest that Ca^{2+} unbinding from the C2 domain would precede membrane unbinding. Ca^{2+} unbinding is not expected to induce a large conformational change,[81] however Ca^{2+} unbinding would alter the electrostatic attraction between the anionic bilayer and the C2 domain, reducing the expected free energy cost for C2 domain unbinding.

A complete description of the unbinding process would therefore include a partial unbinding event where Ca^{2+} unbinds from the C2 domain, and further unbinding would proceed down a reaction coordinate different from the one used here. After unbinding, Loops 1 and 3 would clearly undergo local conformational changes as the Ca^{2+}-binding aspartates are

exposed to each other and to the bilayer surface without the Ca^{2+} ions to neutralize the environment. Due to the slow timescale of Ca^{2+} unbinding and the unbinding-induced local conformational changes near the loop regions, it is impractical to pursue a complete computational description of the unbinding process at this time. Explicitly studying the effect of Ca^{2+} unbinding on the membrane contacts will require follow-on investigations, potentially using a polarizable model which could better represent the charge environment around the Ca^{2+} [82] and a conventional bilayer.

However, we can glean hints on how Ca^{2+} may unbind from the Ca^{2+}-bound unbinding free energy profile and analysis of the underlying simulations. Based on the shape of the free energy profile, Ca^{2+} unbinding is expected to take place after approximately 100 contacts have been broken (Fig. 12), where the profile becomes atter, as it is an easily-accessible state with fewer membrane contacts. These regions correlate with Ca^{2+} accessibility increases, as measured by SASA (Fig. 13), and are representative of a partially unbound state where Ca^{2+} unbinding may take place. Since Syt-1 has fewer membrane contacts in this state, it dissociates more rapidly from the membrane than does Syt-7, whose additional contacts may allow Ca^{2+} to rebind or promote vesicle fusion beyond the duration of cellular Ca^{2+} inux.

Conclusion

Based on the results, we conclude that there is no single interaction that is responsible for the differences in binding kinetics between Syt-1 and Syt-7 C2 domains. Instead, many sequence perturbations in the three loop regions work in concert to cause more membrane contacts to be formed between Syt-7 and the bilayer when compared against Syt-1. These include the addition of extra positive charges and changing lysine residues to the bulkier arginine, which promote stronger electrostatic attraction to and more extensive interaction with anionic phospholipids. The additional electrostatic attraction to the bilayer amplifies the effect of other changes, by for instance causing F167 of Syt-7 to embed deeper into the bilayer than the methionine it replaced in Syt-1 (M173, which is M167 in our relative numbering scheme). In other words, even when the sequence is identical, such as F229 of loop 3, the increased electrostatic attraction serves to increase the membrane contact of these identical residues. With these examples in mind, we hypothesize that these two isoforms evolved from a progenitor Syt, as part of the natural divergence of protein sequences over evolutionary timescales.[83]

The net result of the additional membrane contacts in Syt-7 is an increased cost to unbind from the membrane for Syt-7 C2 domains (Fig. S18). The dissociation discrimination between Syt-1 and Syt-7 fits with their physiological roles, and may be related to the number of vesicles primed at the membrane interface at any one time. Synaptic transmission mediated by Syt-1 is a fast and synchronized process, with many thousands of vesicles all primed to release their contents quickly at the arrival of an action potential. However for any given action potential, only a small fraction fuse with the plasma membrane due to the rapid unbinding of Syt-1, and the size of the readily releasable pool is held approximately constant. The slower unbinding of Syt-7 brought about by the increased membrane contacts permits the smaller pools of other vesicles with less timing-sensitive contents to be released as well, as the time Syt-7 stays bound to the membrane after an Ca^{2+} signal increases to

compensate for the smaller vesicle pool. In this way, the expected number of vesicles released would remain comparable between the two isoforms, despite the different kinetics.

The isolation of residues most closely involved in Syt membrane binding points almost exclusively to residues near the Ca^{2+} binding loops as being critical for membrane binding, including loop 2 residues that have previously not been implicated. Thus we expect that developing a chimeric C2 domain that splices together loops found in Syt-1 and Syt-7 would result in a C2 domain that displays a binding kinetics phenotype intermediate to both Syt-1 and Syt-7. Further engineering to induce additional positive charges near the loops or larger hydrophobic anchors may generate C2 domains that can trigger robust Ca^{2+} mediated fusion at low protein copy numbers.

Supplementary Material

Refer to Web version on PubMed Central for supplementary material.

Acknowledgments

The authors would like to acknowledge Dr. Zhe Wu for helpful insight and discussion, as well as Prof. Jefferson Knight for fruitful discussions and early access to EPR data for Syt-7 C2A.

Funding Information

This research used resources of the National Energy Research Scientific Computing Center (NERSC), which is supported by the Office of Science of the U.S. Department of Energy under Contract No. DE-AC02-05CH11231. Additional simulations were performed using Stampede, hosted at the Texas Advanced Computing Center (TACC) at The University of Texas at Austin through XSEDE (grant number MCA06N060 to E.T.) funded by NSF. J.V.V. acknowledges support from the Sandia National Laboratories Campus Executive Program, which is funded by the Laboratory Directed Research and Development (LDRD) Program. Sandia is a multi-program laboratory managed and operated by Sandia Corporation, a wholly owned subsidiary of Lockheed Martin Corporation, for the US Department of Energy's National Nuclear Security Administration under Contract No. DE-AC04-94AL85000. J.V.V. also acknowledges previous support from the DOE CSGF Fellowship (DE-FG02-97ER25308). This research is also supported by the National Institutes of Health, through grants P41-GM104601 and U54-GM087519 to E.T.

References

1. Xue M, Craig TK, Shin OH, Li L, Brautigam CA, Tomchick DR, Südhof TC, Rosenmund C, Rizo J. Structural and mutational analysis of functional differentiation between synaptotagmins-1 and -7. PLoS One. 2010; 5:1–12.
2. Rizo J, Rosenmund C. Synaptic vesicle fusion. Nat Struct Mol Biol. 2008; 15:665–674. [PubMed: 18618940]
3. Jahn R, Fasshauer D. Molecular machines governing exocytosis of synaptic vesicles. Nature. 2012; 490:201–207. [PubMed: 23060190]
4. Südhof TC. Calcium control of neurotransmitter release. Cold Spring Harbor Perspect Biol. 2012; 4:a011353.
5. Pang ZP, Südhof TC. Cell biology of Ca^{2+}-triggered exocytosis. Curr Opin Cell Biol. 2010; 22:496–505. [PubMed: 20561775]
6. Chapman ER. How does synaptotagmin trigger neurotransmitter release? Annu Rev Biochem. 2008; 77:615–641. [PubMed: 18275379]
7. Südhof TC. Synaptotagmins: Why So Many? J Biol Chem. 2002; 277:7629–7632. [PubMed: 11739399]
8. Brose N, Petrenko AG, Südhof TC, Jahn R. Synaptotagmin: a calcium sensor on the synaptic vesicle surface. Science. 1992; 256:1021–1025. [PubMed: 1589771]

9. Matthew WD, Tsavaler L, Reichardt LF. Identification of a synaptic vesicle-specific membrane protein with a wide distribution in neuronal and neurosecretory tissue. J Cell Biol. 1981; 91:257–269. [PubMed: 7298720]
10. Han W, Rhee JS, Maximov A, Lao Y, Mashimo T, Rosenmund C, Südhof TC. N-Glycosylation Is Essential for Vesicular Targeting of Synaptotagmin 1. Neuron. 2004; 41:85–99. [PubMed: 14715137]
11. Maximov A, Südhof TC. Autonomous function of synaptotagmin 1 in triggering synchronous release independent of asynchronous release. Neuron. 2005; 48:547–554. [PubMed: 16301172]
12. Schonn JS, Maximov A, Lao Y, Südhof TC, Sørensen JB. Synaptotagmin-1 and -7 are functionally overlapping Ca^{2+} sensors for exocytosis in adrenal chromaffin cells. Proc Natl Acad Sci USA. 2008; 105:3998–4003. [PubMed: 18308932]
13. Gustavsson N, Lao Y, Maximov A, Chuang JC, Kostromina E, Repa JJ, Li C, Radda GK, Südhof TC, Han W. Impaired insulin secretion and glucose intolerance in synaptotagmin-7 null mutant mice. Proc Natl Acad Proc Natl Acad Sci USA. 2008; 105:3992–3997. [PubMed: 18308938]
14. Gustavsson N, Wei SH, Hoang DN, Lao Y, Zhang Q, Radda GK, Rorsman P, Südhof TC, Han W. Synaptotagmin-7 is a principal Ca^{2+} sensor for Ca^{2+}-induced glucagon exocytosis in pancreas. J Physiol. 2009; 587:1169–1178. [PubMed: 19171650]
15. Bacaj T, Wu D, Yang X, Morishita W, Zhou P, Xu W, Malenka R, Südhof T. Synaptotagmin-1 and Synaptotagmin-7 Trigger Synchronous and Asynchronous Phases of Neurotransmitter Release. Neuron. 2013; 80:947–959. [PubMed: 24267651]
16. Weber JP, Toft-Bertelsen TL, Mohrmann R, Delgado-Martinez I, Sørensen JB. Synaptotagmin-7 Is an Asynchronous Calcium Sensor for Synaptic Transmission in Neurons Expressing SNAP-23. PLoS One. 2014; 9:e114033. [PubMed: 25422940]
17. Brandt DS, Coffman MD, Falke JJ, Knight JD. Hydrophobic contributions to the membrane docking of synaptotagmin 7 C2A domain: mechanistic contrast between isoforms 1 and 7. Biochemistry. 2012; 51:7654–7664. [PubMed: 22966849]
18. Ohkubo YZ, Pogorelov TV, Arcario MJ, Christensen GA, Tajkhorshid E. Accelerating Membrane Insertion of Peripheral Proteins with a Novel Membrane Mimetic Model. Biophys J. 2012; 102:2130–2139. [PubMed: 22824277]
19. Vermaas JV, Tajkhorshid E. A Microscopic View of Phospholipid Insertion into Biological Membranes. J Phys Chem B. 2014; 118:1754–1764. [PubMed: 24313792]
20. Pogorelov TV, Vermaas JV, Arcario MJ, Tajkhorshid E. Partitioning of Amino Acids into a Model Membrane: Capturing the Interface. J Phys Chem B. 2014; 118:1481–1492. [PubMed: 24451004]
21. Baylon JL, Lenov IL, Sligar SG, Tajkhorshid E. Characterizing the Membrane-Bound State of Cytochrome P450 3A4: Structure, Depth of Insertion, and Orientation. J Am Chem Soc. 2013; 135:8542–8551. [PubMed: 23697766]
22. Vermaas JV, Tajkhorshid E. Conformational heterogeneity of α-synuclein in membrane. Biochim Biophys Acta Biomembr. 2014; 1838:3107–3117.
23. Arcario MJ, Tajkhorshid E. Membrane-Induced Structural Rearrangement and Identification of a Novel Membrane Anchor in Talin F2F3. Biophys J. 2014; 107:2059– 2069. [PubMed: 25418091]
24. Baylon JL, Vermaas JV, Muller MP, Arcario MJ, Pogorelov TV, Tajkhorshid E. Atomic-level description of protein-lipid interactions using an accelerated membrane model. Biochim Biophys Acta Biomembr. 2016; 1858:1573–1583.
25. Zhang L, Rajendram M, Weibel DB, Yethiraj A, Cui Q. Ionic Hydrogen Bonds and Lipid Packing Defects Determine the Binding Orientation and Insertion Depth of RecA on Multicomponent Lipid Bilayers. J Phys Chem B. 2016; 120:8424–8437. [PubMed: 27095675]
26. Wu Z, Schulten K. Synaptotagmin's Role in Neurotransmitter Release Likely Involves Ca^{2+}-induced Conformational Transition. Biophys J. 2014; 107:1156–1166. [PubMed: 25185551]
27. Sugita Y, Kitao A, Okamoto Y. Multidimensional replica-exchange method for free-energy calculations. J Chem Phys. 2000; 113:6042–6051.
28. Boettcher JM, Davis-Harrison RL, Clay MC, Nieuwkoop AJ, Ohkubo YZ, Tajkhorshid E, Morrissey JH, Rienstra CM. Atomic View of Calcium-Induced Clustering of Phosphatidylserine in Mixed Lipid Bilayers. Biochemistry. 2011; 50:2264–2273. [PubMed: 21294564]

29. Leventis PA, Grinstein S. The Distribution and Function of Phosphatidylserine in Cellular Membranes. Annu Rev Biophys. 2010; 39:407–427. [PubMed: 20192774]
30. Zhang Y, Tang T, Girit C, Hao Z, Martin M, Zettl A, Crommie MF, Shen YR, Weng F. Direct Observation of a Widely Tunable Bandgap in Bilayer Graphene. Nature. 2009; 459:820–823. [PubMed: 19516337]
31. Fernandez I, Araç D, Ubach J, Gerber SH, Shin OH, Gao Y, Anderson RGW, Südhof TC, Rizo J. Three-dimensional structure of the synaptotagmin 1 C2B-domain: Synaptotagmin 1 as a phospholipid binding machine. Neuron. 2001; 32:1057–1069. [PubMed: 11754837]
32. Best RB, Zhu X, Shim J, Lopes PEM, Mittal J, Feig M, MacKerell AD. Optimization of the Additive CHARMM All-Atom Protein Force Field Targeting Improved Sampling of the Backbone ϕ, ψ and Side-Chain χ_1 and χ_2 Dihedral Angles. J Chem Theory Comput. 2012; 8:3257–3273. [PubMed: 23341755]
33. MacKerell AD Jr, Feig M, Brooks CL III. Improved treatment of the protein backbone in empirical force fields. J Am Chem Soc. 2004; 126:698–699. [PubMed: 14733527]
34. Bacaj T, Wu D, Yang X, Morishita W, Zhou P, Xu W, Malenka RC, Südhof TC. Synaptotagmin-1 and Synaptotagmin-7 Trigger Synchronous and Asynchronous Phases of Neurotransmitter Release. Neuron. 2013; 80:947–959. [PubMed: 24267651]
35. Helmchen F, Borst J, Sakmann B. Calcium dynamics associated with a single action potential in a CNS presynaptic terminal. Biophys J. 1997:72.
36. Jo S, Kim T, Iyer VG, Im W. CHARMM-GUI: A Web-Based Graphical User Interface for CHARMM. J Comp Chem. 2008; 29:1859–1865. [PubMed: 18351591]
37. Jo S, Lim JB, Klauda JB, Im W. CHARMM-GUI membrane builder for mixed bilayers and its application to yeast membranes. Biophys J. 2009; 97:50–58. [PubMed: 19580743]
38. Wu EL, Cheng X, Jo S, Rui H, Song KC, Dávila-Contreras EM, Qi Y, Lee J, Monje-Galvan V, Venable RM, Klauda JB, Im W. CHARMM-GUI Membrane Builder toward realistic biological membrane simulations. J Comput Chem. 2014; 35:1997–2004. [PubMed: 25130509]
39. Jurkiewicz P, Cwiklik L, Vojtíšková A, Jungwirth P, Hof M. Structure, dynamics, and hydration of POPC/POPS bilayers suspended in NaCl, KCl, and CsCl solutions. Biochim Biophys Acta - Biomembr. 2012; 1818:609–616.
40. Vermaas JV, Baylon JL, Arcario MJ, Muller MP, Wu Z, Pogorelov TV, Tajkhorshid E. Efficient Exploration of Membrane-Associated Phenomena at Atomic Resolution. J Membr Biol. 2015; 248:563–582. [PubMed: 25998378]
41. Humphrey W, Dalke A, Schulten K. VMD – Visual Molecular Dynamics. J Mol Graphics. 1996; 14:33–38.
42. Phillips JC, Braun R, Wang W, Gumbart J, Tajkhorshid E, Villa E, Chipot C, Skeel RD, Kale L, Schulten K. Scalable Molecular Dynamics with NAMD. J Comp Chem. 2005; 26:1781–1802. [PubMed: 16222654]
43. Klauda JB, Venable RM, Freites JA, O'Connor JW, Tobias DJ, Mondragon-Ramirez C, Vorobyov I, MacKerell AD Jr, Pastor RW. Update of the CHARMM all-atom additive force field for lipids: Validation on six lipid types. J Phys Chem B. 2010; 114:7830–7843. [PubMed: 20496934]
44. Jorgensen WL, Chandrasekhar J, Madura JD, Impey RW, Klein ML. Comparison of simple potential functions for simulating liquid water. J Chem Phys. 1983; 79:926–935.
45. Darden T, York D, Pedersen LG. Particle mesh Ewald: An $N\cdot\log(N)$ method for Ewald sums in large systems. J Chem Phys. 1993; 98:10089–10092.
46. Essmann U, Perera L, Berkowitz ML, Darden T, Lee H, Pedersen LG. A smooth particle mesh Ewald method. J Chem Phys. 1995; 103:8577–8593.
47. Martyna GJ, Tobias DJ, Klein ML. Constant Pressure Molecular Dynamics Algorithms. J Chem J Chem Phys. 1994; 101:4177–4189.
48. Feller SE, Zhang Y, Pastor RW, Brooks BR. Constant pressure molecular dynamics simulation: The Langevin piston method. J Chem Phys. 1995; 103:4613–4621.
49. Sheinerman FB, Brooks CL III. Calculations on folding of segment B1 of streptococcal protein G. J Mol Biol. 1998; 278:439–456. [PubMed: 9571063]

50. Fukunishi H, Watanabe O, Takada S. On the Hamiltonian replica exchange method for efficient sampling of biomolecular systems: Application to protein structure prediction. J Chem Phys. 2002; 116:9058–9067.
51. Moradi M, Tajkhorshid E. Mechanistic picture for conformational transition of a membrane transporter at atomic resolution. Proc Natl Acad Sci USA. 2013; 110:18916–18921. [PubMed: 24191018]
52. Moradi M, Tajkhorshid E. Computational recipe for efficient description of large-scale conformational changes in biomolecular systems. J Chem Theory Comput. 2014; 10:2866–2880. [PubMed: 25018675]
53. Filipe HAL, Moreno MJ, Róg T, Vattulainen I, Loura LMS. How to tackle the issues in free energy simulations of long amphiphiles interacting with lipid membranes: Convergence and local membrane deformations. J Phys Chem B. 2014; 118:3572–3581. [PubMed: 24635540]
54. Fiorin G, Klein ML, Hénin J. Using collective variables to drive molecular dynamics simulations. Mol Phys. 2013; 111:3345–3362.
55. Amdahl G. Validity of the single-processor approach to achieving large scale computing capabilities. AFIPS Conf Proc. 1967; 30:483–485.
56. Sabri Dashti D, Roitberg AE. Optimization of umbrella sampling replica exchange molecular dynamics by replica positioning. J Chem Theory Comput. 2013; 9:4692–4699. [PubMed: 26583388]
57. Jiang W, Luo Y, Maragliano L, Roux B. Calculation of free energy landscape in multi-dimensions with hamiltonian-exchange umbrella sampling on petascale supercomputer. J Chem Theory Comput. 2012; 8:4672–4680. [PubMed: 26605623]
58. Habeck M. Bayesian estimation of free energies from equilibrium simulations. Phys Rev Lett. 2012:109.
59. Bartels C. Analyzing biased Monte Carlo and molecular dynamics simulations. Chem Phys Lett. 2000; 331:446–454.
60. Moradi M, Tajkhorshid E. Computational recipe for efficient description of large-scale conformational changes in biomolecular systems. J Chem Theory Comput. 2014; 10:2866–2880. [PubMed: 25018675]
61. Kumar S, Bouzida D, Swendsen RH, Kollman PA, Rosenberg JM. The Weighted Histogram Analysis Method for Free-Energy Calculations on Biomolecules. I. The Method. J Comp Chem. 1992; 13:1011–1021.
62. Massey FJ. The Kolmogorov-Smirnov Test for Goodness of Fit. J Am Stat Assoc. 1951; 46:68.
63. Limentani GB, Ringo MC, Ye F, Bergquist ML, McSorley EO. Beyond the t-Test: Statistical Equivalence Testing. Analyt Chem. 2005; 77:221A–226A.
64. Frazier AA, Roller CR, Havelka JJ, Hinderliter A, Cafiso DS. Membrane-Bound Orientation and Position of the Synaptotagmin I C2A Domain by Site-Directed Spin Labeling. Biochemistry. 2003; 42:96–105. [PubMed: 12515543]
65. Rufener E, Frazier AA, Wieser CM, Hinderliter A, Cafiso DS. Membrane-bound orientation and position of the synaptotagmin C2B domain determined by sitedirected spin labeling. Biochemistry. 2005; 44:18–28. [PubMed: 15628842]
66. Osterberg JR, Chon NL, Boo A, Maynard FA, Lin H, Knight JD. Membrane Docking of the Synaptotagmin 7 C2A Domain: Electron Paramagnetic Resonance Measurements Show Contributions from Two Membrane Binding Loops. Biochemistry. 2015; 54:5684–5695. [PubMed: 26322740]
67. Malmberg NJ, Falke JJ. Use of EPR power saturation to analyze the membrane-docking geometries of peripheral proteins: applications to C2 domains. Annu Rev Biophys Biomol Struct. 2005; 34:71–90. [PubMed: 15869384]
68. Chon NL, Osterberg JR, Henderson J, Khan HM, Reuter N, Knight JD, Lin H. Membrane Docking of the Synaptotagmin 7 C2A Domain: Computation Reveals Interplay between Electrostatic and Hydrophobic Contributions. Biochemistry. 2015; 54:5696–5711. [PubMed: 26333120]
69. Herrick DZ, Kuo W, Huang H, Schwieters CD, Ellena JF, Cafiso DS. Solution and Membrane-Bound Conformations of the Tandem C2A and C2B Domains of Synaptotagmin 1: Evidence for Bilayer Bridging. J Mol Biol. 2009; 390:913–923. [PubMed: 19501597]

70. Fuson KL, Montes M, Robert JJ, Sutton RB. Structure of human synaptotagmin 1 C2AB in the absence of Ca^{2+} reveals a novel domain association. Biochemistry. 2007; 46:13041–13048. [PubMed: 17956130]
71. Herrick DZ, Sterbling S, Rasch KA, Hinderliter A, Cafiso DS. Position of synaptotagmin I at the membrane interface: Cooperative interactions of tandem C2 domains. Biochemistry. 2006; 45:9668–9674. [PubMed: 16893168]
72. Bai H, Xue R, Bao H, Zhang L, Yethiraj A, Cui Q, Chapman ER. Different states of synaptotagmin regulate evoked versus spontaneous release. Nat Commun. 2016; 7:10971. [PubMed: 27001899]
73. Liu H, Bai H, Xue R, Takahashi H, Edwardson JM, Chapman ER. Linker mutations reveal the complexity of synaptotagmin 1 action during synaptic transmission. Nat Nat Neurosci. 2014; 17:670–677. [PubMed: 24657966]
74. Vasquez JK, Chantranuvatana K, Giardina DT, Coffman MD, Knight JD. Lateral Diffusion of Proteins on Supported Lipid Bilayers: Additive Friction of Synaptotagmin 7 C2AC2B Tandem Domains. Biochemistry. 2014; 53:7904–7913. [PubMed: 25437758]
75. Bai J, Tucker WC, Chapman ER. PIP2 increases the speed of response of synaptotagmin and steers its membrane-penetration activity toward the plasma membrane. Nat Struct Mol Biol. 2004; 11:36–44. [PubMed: 14718921]
76. Davis AF, Bai J, Fasshauer D, Wolowick MJ, Lewis JL, Chapman ER. Kinetics of synaptotagmin responses to Ca^{2+} and assembly with the core SNARE complex onto membranes. Neuron. 1999; 24:363–376. [PubMed: 10571230]
77. Wu Z, Cui Q, Yethiraj A. Why Do Arginine and Lysine Organize Lipids Differently? Insights from Coarse-Grained and Atomistic Simulations. J Phys Chem B. 2013; 117:12145–12156. [PubMed: 24024591]
78. Li L, Vorobyov I, Allen TW. The different interactions of lysine and arginine side chains with lipid membranes. J Phys Chem B. 2013; 117:11906–11920. [PubMed: 24007457]
79. Sugita S, Shin OH, Han W, Lao Y, Südhof TC. Synaptotagmins form a hierarchy of exocytotic Ca^{2+} sensors with distinct Ca^{2+} affinities. EMBO J. 2002; 21:270–280. [PubMed: 11823420]
80. Nalefski EA, Wisner MA, Chen JZ, Sprang SR, Fukuda M, Mikoshiba K, Falke JJ. C2 domains from different Ca^{2+} signaling pathways display functional and mechanistic diversity. Biochemistry. 2001; 40:3089–3100. [PubMed: 11258923]
81. Shao X, Fernandez I, Südhof TC, Rizo J. Solution structures of the Ca^{2+}-free and Ca^{2+}-bound C2A domain of synaptotagmin I: Does Ca^{2+} induce a conformational change? Biochemistry. 1998; 37:16106–16115. [PubMed: 9819203]
82. Li H, Ngo V, Da Silva MC, Salahub DR, Callahan K, Roux B, Noskov SY. Representation of IonProtein Interactions Using the Drude Polarizable Force-Field. J Phys Chem B. 2015; 119:9401–9416. [PubMed: 25578354]
83. Povolotskaya IS, Kondrashov FA. Sequence space and the ongoing expansion of the protein universe. Nature. 2010; 465:922–926. [PubMed: 20485343]

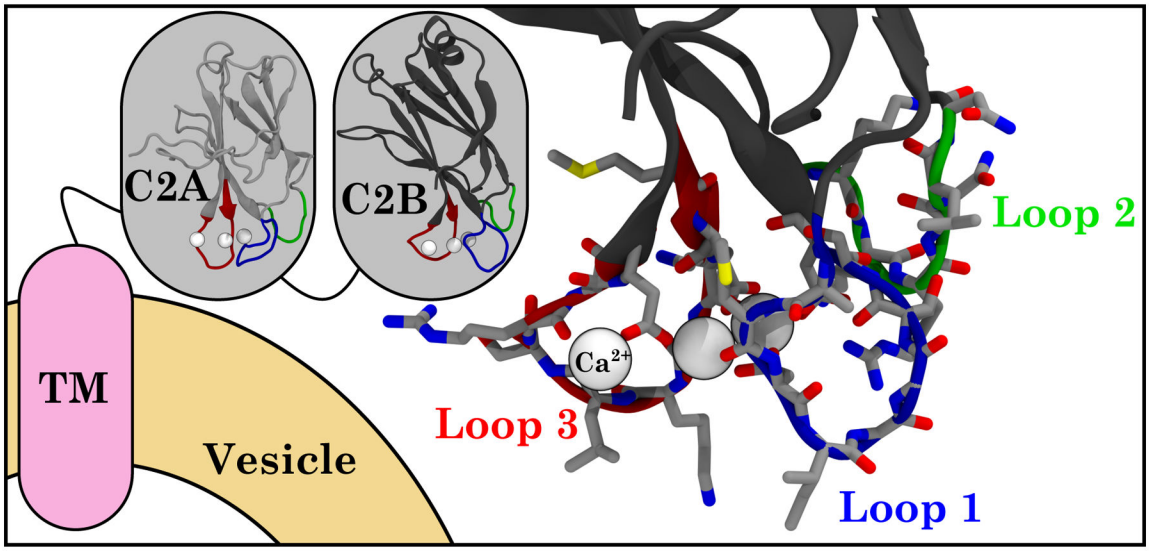

Figure 1.

Schematic of Synaptotagmin structure. Most Synaptotagmin (Syt) isoforms consist of three major elements, a transmembrane domain (TM, pink), and two C2 domains, C2A and C2B (gray), which are connected by short linkers. The C2 domains share the same overall structure, with predominantly sheet-like secondary structure, and three loops (blue, green, and red for Loops 1–3, respectively) actively involved in coordinating Ca^{2+} (white spheres). The structures shown within the schematic are the C2A and C2B domains from Syt-7 (PDB: 2D8K, and 3N5A[1]), with a close-up view of the Ca^{2+}-binding loops from C2B.

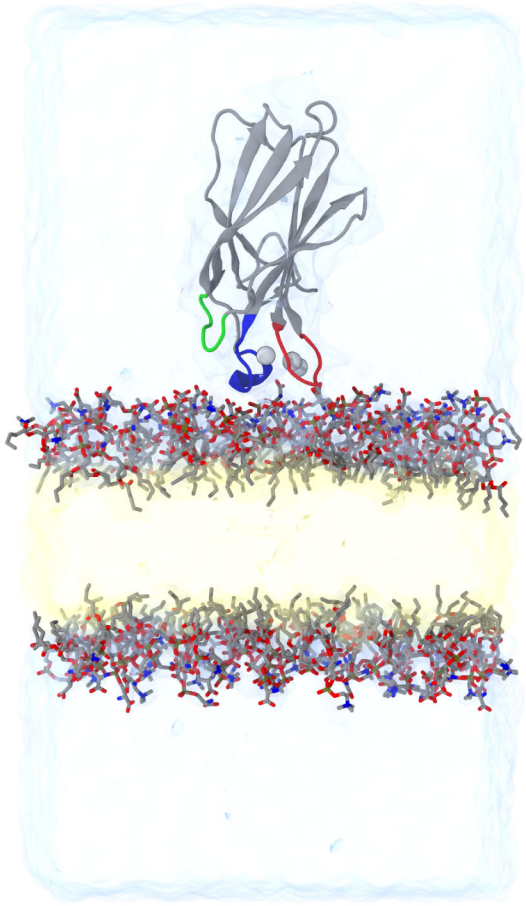

Figure 2.

An example of an initial simulation setup, specifically Syt-1 C2A. As shown, each protein (gray cartoon with blue, green, and red highlights for Loops 1–3) was placed above a HMMM bilayer with a 1:1 ratio of PS:PC head groups (sticks) with a 1,1-dichloroethane core (yellow surface) and surrounding water and ions (blue surface). Ca^{2+} ions (white outlined spheres) were added to structures as required.

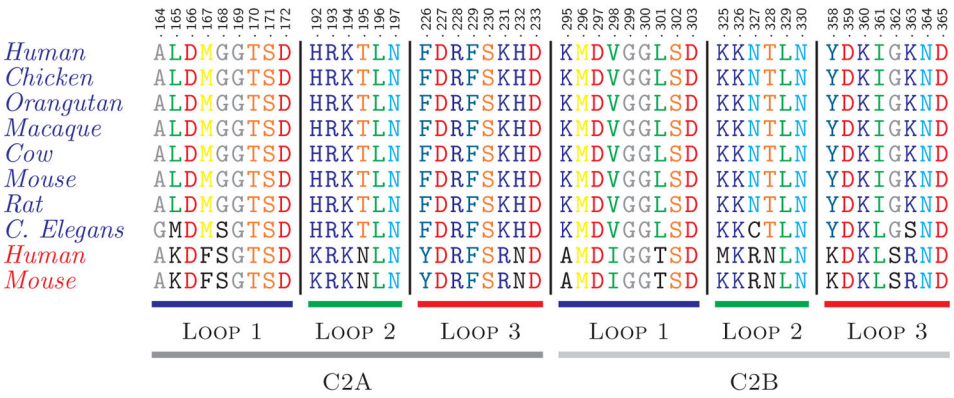

Figure 3.

Loop definitions for Loops 1–3 of Syt isoforms, including their sequences across many different species. Syt-1 sequences are labeled in blue, while those from Syt-7 are labeled in red. The labeled loops use a numbering scheme based on their alignment to the sequence of human Syt-7.

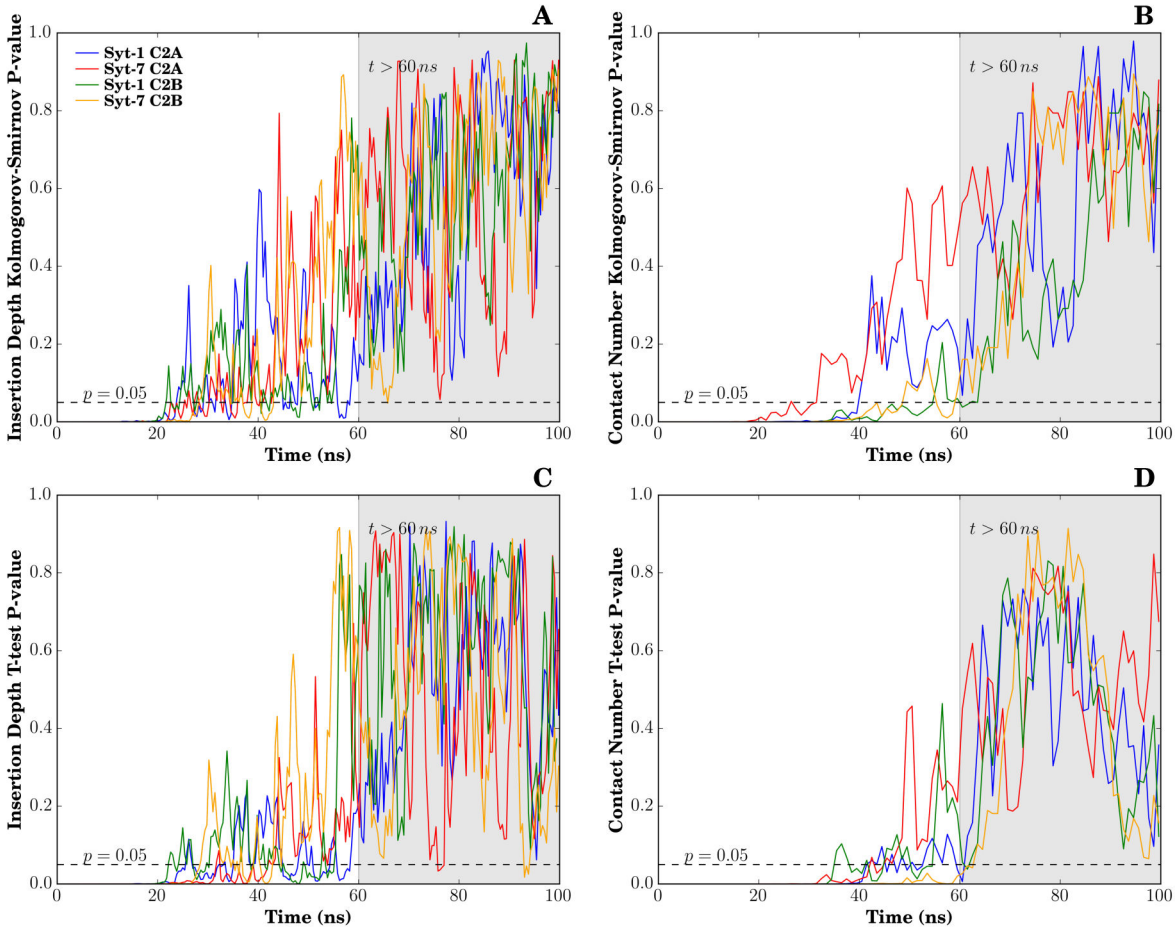

Figure 4.

Statistical comparison for the distribution of insertion depth (A & C) and contact number (B & D) for all 20 binding trajectories. (A & B) compare using the Kolmogorov-Smirnov statistic, which compares the distribution at a given time with the distribution at the end of the simulations. When $p < 0.05$, we can say with 95% confidence that the distribution at time t differs from the observed distribution at the end of simulation. (C & D) compare the distribution at a given time to the mean distribution over the last 20 ns using two one-sided T-test (TOST), which can discriminate if two distributions are equal. Here when $p < 0.05$, we can say with 95% confidence that the distribution at a given time has a mean that differs by less than a cutoff from the reference distribution. In this case, the cutoff is chosen to be one standard deviation from the reference distribution, taken from the last 20 ns of simulation. With few exceptions, the statistic shows that when $t > 60$ ns the distribution of the two observables we are most interested in are similar, and is the basis for why we choose to analyze equilibrium properties when $t > 60$ ns.

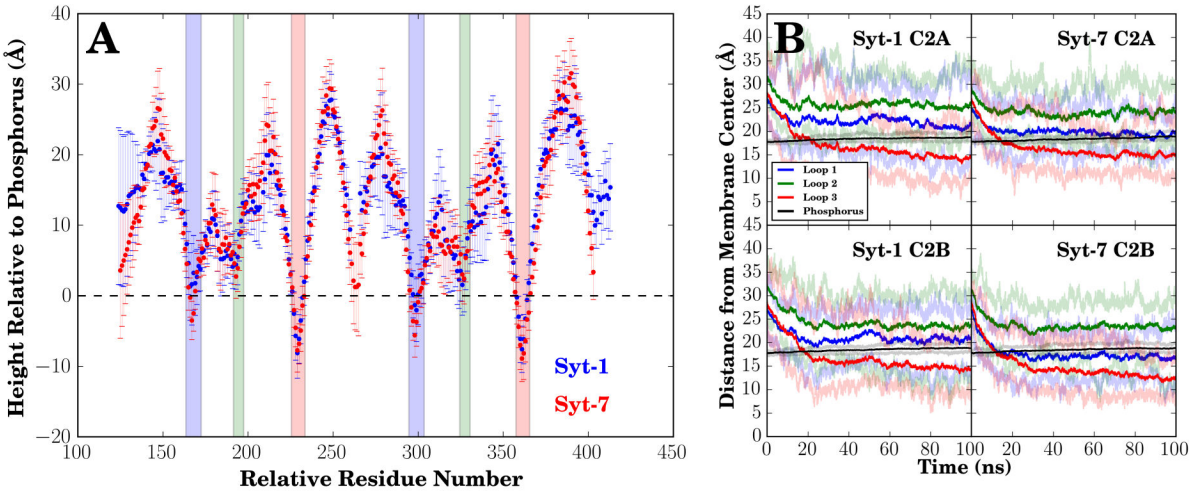

Figure 5.

Syt membrane insertion depths. (A) Mean per residue height from the membrane, as measured by the position of the residue's α-carbon relative to the mean plane of the membrane phosphorus atoms. The relative residue numbers are with respect to the generalized Syt sequence, with the respective C2 domain loops highlighted. Here, blue points are for Syt-1, red points are for Syt-7, with the error bars representing the standard deviation observed for each residue. (B) Mean penetration depth time series, as measured by the position of the center of mass of each loop, including side chains. The mean position of the membrane phosphorus groups is shown for contrast (black line). The mean depth over the last 40 ns of the 100 ns trajectory are reported in Table 2. Lighter colored lines above and below the darker mean line represent the minimum and maximum insertion depth observed over all 20 replicates. Colors signifying each loop are consistent across both panels, Loops 1–3 are blue, green, and red, respectively.

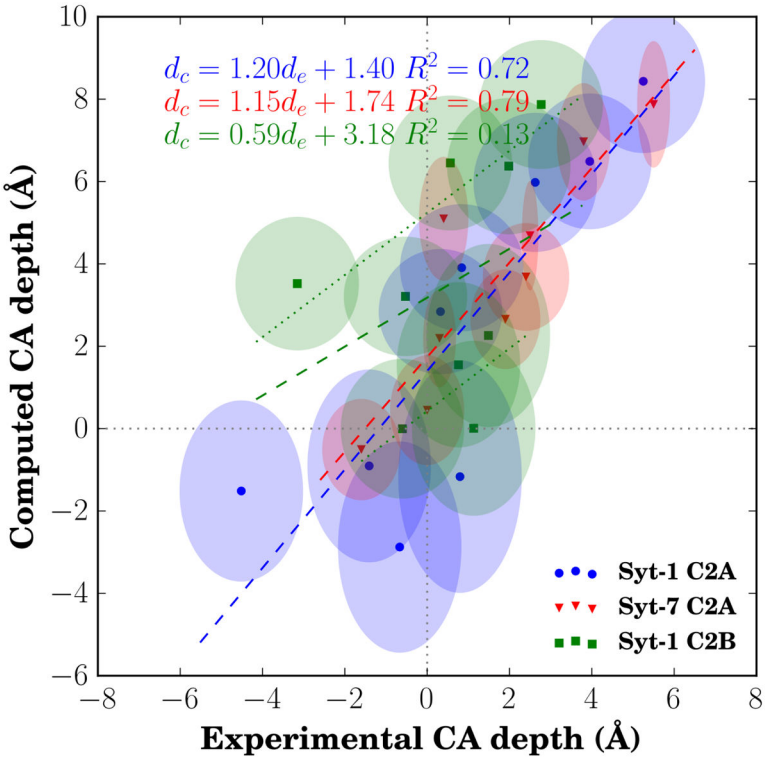

Figure 6.

Comparison of the mean membrane penetration depths relative to phosphorus determined over the last 40 ns of HMMM simulations (y-axis) and available experimental results (x-axis). The determined datapoints are for the α-carbons of relative residues 166–169 (square markers) and 227–231 (circle markers), which are in loops 1 and 3 respectively. Comparison data for Syt-1 C2A (blue), Syt-7 C2A (red) and Syt-1 C2B (green) were taken from the membrane-bound models consistent with site-directed spin labeling experiments.[64–66] The estimated error for each point is represented by a semitransparent ellipse, whose width and height correspond to the reported uncertainty or standard deviation for experimental and computed depths, respectively. The trendline, calculated as a linear regression from the individual comparison sets, is reported as both a dashed line along with its equation. The subtrends for Loops 1 and 3 independently within Syt-1 C2B are reported as two green dotted lines.

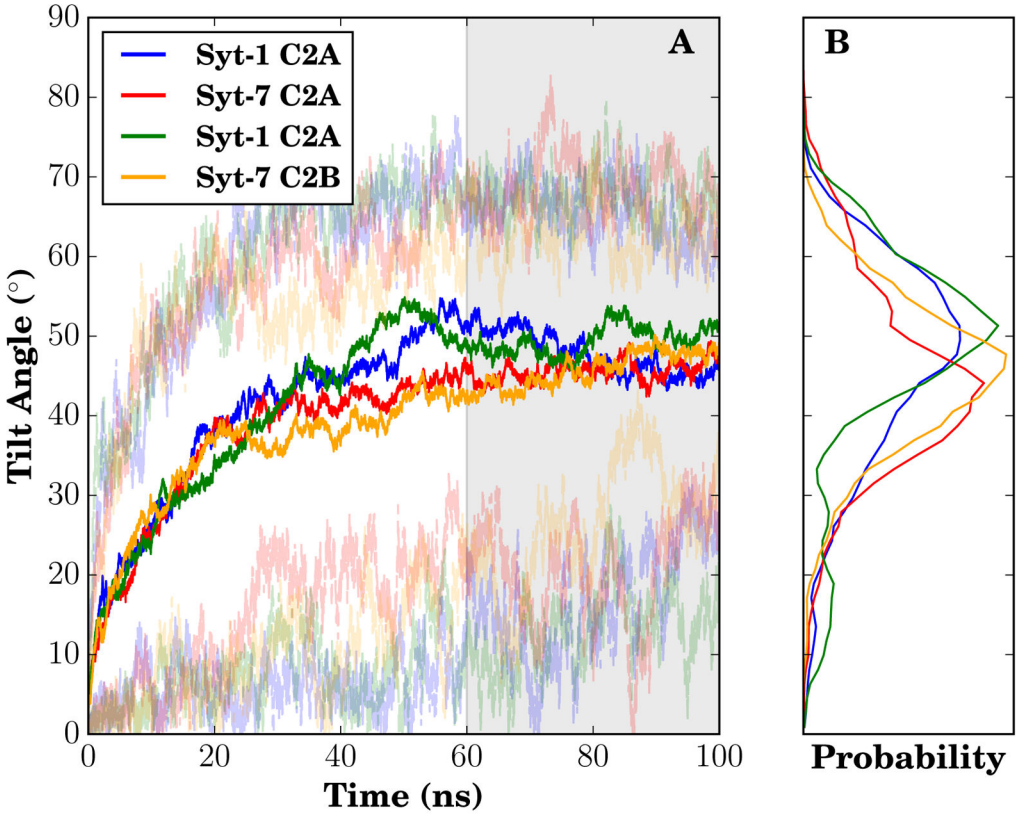

Figure 7.

Syt orientation change upon membrane binding. (A) Time series of the mean (dark line), minimum, and maximum (light lines) tilt angle of C2 domains. A tilt angle of 0° is the initial state when the long axis of the C2 domain is co-linear with the membrane normal, and 90° would represent a C2 domain lying along the face of the membrane. (B) Distribution of tilt angles over the last 40 ns of the trajectories (highlighted in gray in (A)) for all 20 simulations. Each separate isoform has its own color: blue and green for the C2A and C2B domains of Syt-1, and red and orange for the C2A and C2B domains of Syt-7.

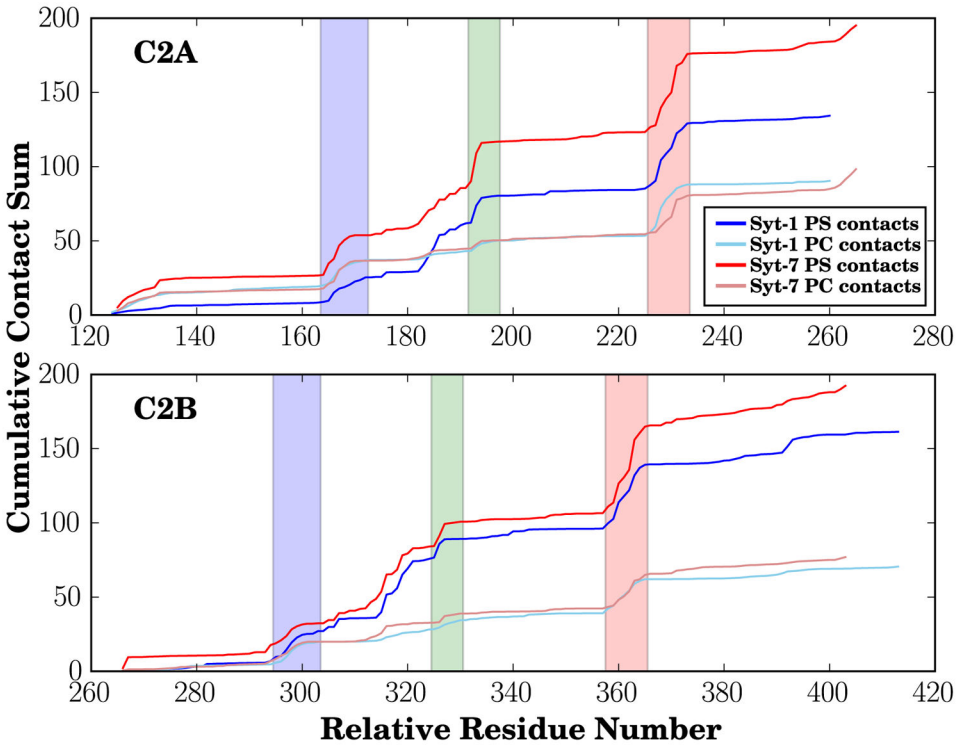

Figure 8.

Cumulative contacts between C2A and C2B domains and respective membrane components. Eq. (1) describes the contact definition. Sections of the C2 domains corresponding to Loops 1, 2, and 3 are highlighted in blue, green, and red, respectively. The precise number of contacts contributed by each loop is enumerated in Table S3.

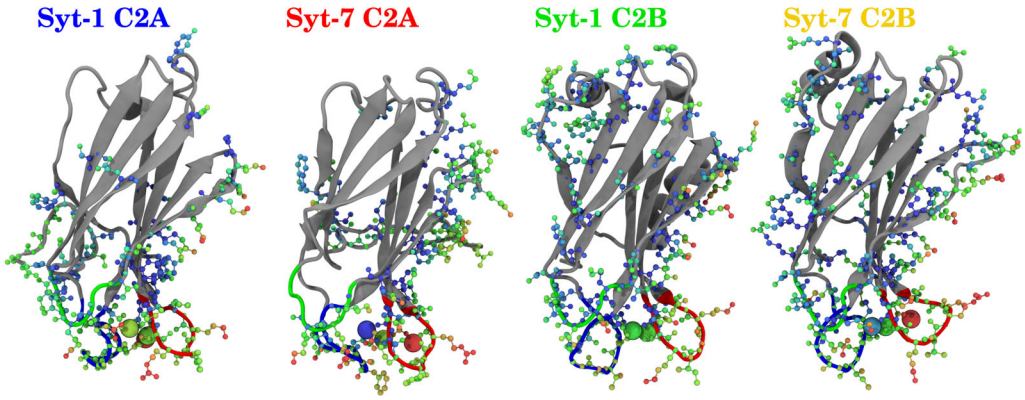

Figure 9.

Contact visualization for the four C2 domains. Each C2 domain is shown as a gray cartoon representation, with the three loop regions colored in blue, green, and red respectively. Protein residues that make contacts with the membrane are shown in a ball and stick representation, where individual heavy atoms are colored according to the number of contacts formed, with redder colors forming more contacts than bluer colors. Similarly, Ca^{2+} ions are shown as spheres utilizing the same coloration. Animations to assist in seeing depth are available as Supporting Information, as are structure files with PS and PC contacts stored in the beta and occupancy fields, respectively.

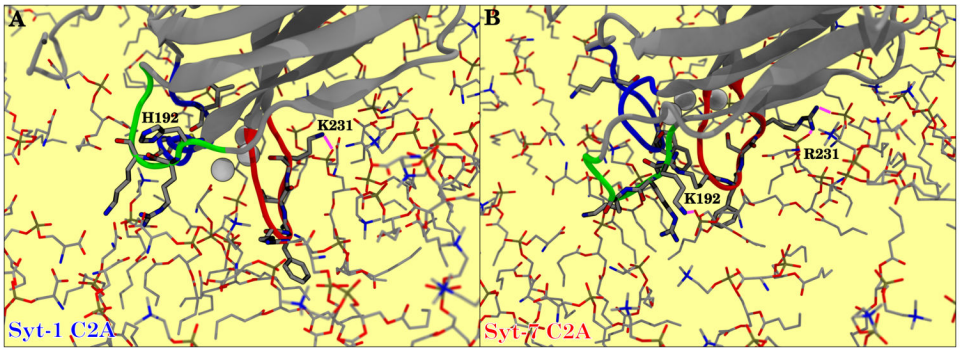

Figure 10.

Top views of snapshots of Syt-1 C2A (A) and Syt-7 C2A (B) highlighting key differences in the binding interaction. The C2A domains are drawn in a gray cartoon, except in Loops 1–3, which are blue, green, and red, respectively. Sidechains of relative residues 165, 167, 168, 192–194, and 228–231 are drawn in outlined stick representations, while nearby HMMM phospholipids are drawn similarly but without an outline. Specific interactions that differ between Syt-1 and Syt-7 and lipids are highlighted with pink lines to represent a hydrogen bond formed between the two heavy atoms. Specifically, the sequence differences between relative residues 192 and 231 induce different interaction patterns. Ca^{2+} ions are the outlined white spheres. All hydrogens have been omitted for clarity, and the DCLE molecules are represented by the yellow background.

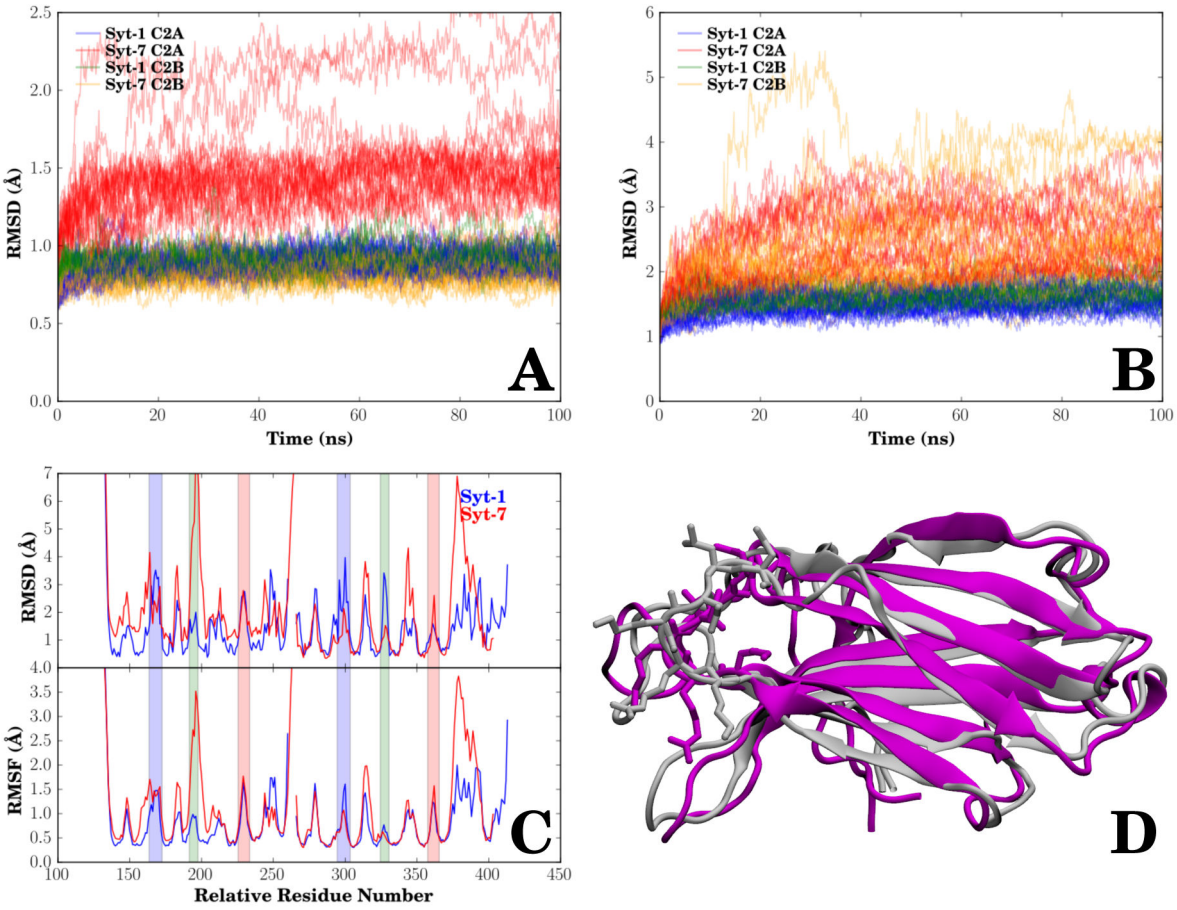

Figure 11.

(A) RMSD of the C2 domain β-sheet backbone atoms along the trajectories, with all 20 trajectories represented by their own semi-transparent line colorcoded according to C2 domain (blue for Syt-1 C2A, red for Syt-7 C2A, green for Syt-1 C2B, and orange for Syt-7 C2B). (B) RMSD of the full C2 domain backbone along the trajectories, with all 20 trajectories represented by their own semi-transparent line colorcoded according to C2 domain using the same colorscheme as in A. (C) Per residue RMSD and root mean square uctuation (RMSF) measured for the α-carbons of the backbone averaged over the last 40 ns of trajectory for Syt-1 (blue) and Syt-7 (red). Residues corresponding to Loops 1–3 are highlighted with blue, green, and red semi-transparent backgrounds for both C2A and C2B domains. (D) Structural comparison of a simulation structure (gray) and the original NMR structure used for model construction (purple). Heavy atoms of residues in Loop 2 are shown in a stick representation, with the rest of the protein shown as a cartoon for context.

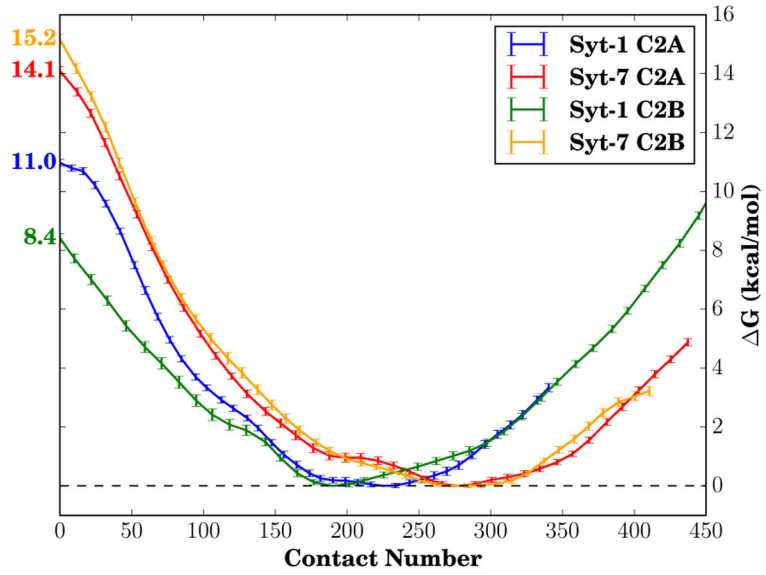

Figure 12.

Unbinding free energy profiles for Syt-1 and Syt-7 C2 domains. The reaction coordinate used is the contact definition optimized for computational speed (Eq. 2). The profiles are adjusted with their minimum set to 0, so that the labeled values at no contacts are the unbinding free energies for the respective C2 domains. Each profile is colored according to the C2 domain: Syt-1 C2A and C2B domains are blue and green respectively, while the corresponding lines for Syt-7 are red and orange. The displayed errorbars are the statistical error from subset sampling. For an alternative convergence analysis, see Fig. S17.

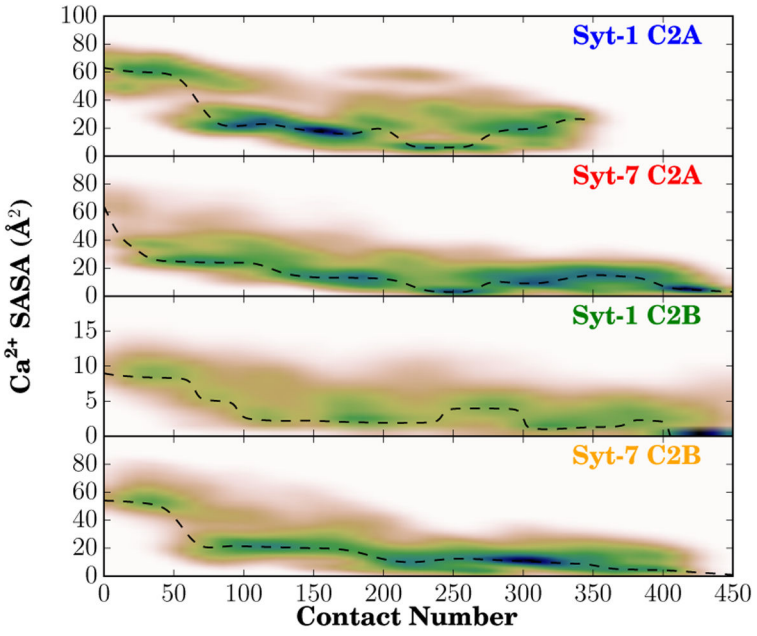

Figure 13.

Solvent accessible surface area (SASA) distribution of the bound Ca^{2+} ions bound to the C2 domains as a function of contact number during the REUS calculations. The SASA was calculated using VMD,[41] and excludes Ca^{2+} contact surface with protein or lipid within a 1.4 Å probe radius. The dotted line follows the maxima within the distribution as a function of contact number.

Table 1

Starting C2 structures used for membrane-binding simulations, including the number of bound Ca^{2+} ions.

C2 domain	PDBID	Species	Ca^{2+}
Syt-1 C2A	3F04	Human	3
Syt-1 C2B	1K5W	Rat	2
Syt-7 C2A	2D8K	Human	3
Syt-7 C2B	3N5A	Mouse	3

Table 2

Mean penetration depth (in Å) over the trajectory when $t > 60$ ns, measured as the position of the center of mass of each loop region, including side chains, relative to the average membrane phosphorus height. This is directly comparable with Fig. 5B, with the exception of the "overall" column, which should be compared with Figs. S1–S4. The overall column monitors the mean of the deepest loop penetration at any one time, the identity of which differs depending on the simulation. The uncertainty in the last digit is reported in parenthesis.

		Overall	Loop 1	Loop 2	Loop 3
Syt-1	C2A	4.0(1)	−1.4(1.6)	−5.6(1.6)	4.8(8)
	C2B	3.9(1)	−2.0(4)	−4.7(4)	4.2(4)
Syt-7	C2A	4.3(1)	−0.3(5)	−5.2(6)	3.9(4)
	C2B	5.9(1)	2.4(1.1)	−4.5(8)	6.4(6)